Sulfur dioxide removal by calcium-modified fibrous KCC-1 mesoporous silica: kinetics, thermodynamics, isotherm and mass transfer mechanism

Muhammad Adli Hanif[1] · Naimah Ibrahim[1] · Khairuddin Md. Isa[2] · Umi Fazara Md. Ali[2] · Tuan Amran Tuan Abdullah[3] · Aishah Abdul Jalil[3]

Abstract

The removal of sulfur dioxide from industrial flue gas through dry flue gas desulfurization method commonly involves the use of adsorption process with porous sorbent. The efficiency of this process is highly dependent on the adsorption capacity and the adsorption rate of SO_2 onto the sorbent materials. The use of KCC-1 mesoporous silica modified with calcium metal additives (Ca/KCC-1) in SO_2 adsorption is examined in a fixed bed reactor system. The adsorption capacity of Ca/KCC-1 is found to be critically governed by the reaction temperature and inlet SO_2 concentration where low values of both parameters are favorable to achieve the highest adsorption capacity of 3241.94 mg SO_2/g sorbent. SO_2 molecules are adsorbed on the surface of Ca/KCC-1 by both physisorption and chemisorption processes as assumed by the Avrami kinetic model. Thermodynamic study shows that the process is exothermic and spontaneous in nature, and changes from an ordered stage on the surface of KCC-1 towards an increasingly random stage. The process is well explained by Freundlich isotherm model indicating a slightly heterogeneous process and moderate adsorption capacity. The adsorption stage is limited by film diffusion at the initial stage and by intraparticle diffusion during the transfer of SO_2 into the network of pores before adsorption takes place on the active sites.

Keywords KCC-1 mesoporous silica · SO_2 adsorption · Kinetics · Thermodynamics · Isotherm · Mass transfer mechanism

1 Introduction

Dry flue gas desulfurization (FGD) is a prominent method in tackling issues regarding emissions of sulfur containing gases e.g., SO_2, H_2S, into the atmosphere. This method is favored mainly due to their high removal efficiency, lack of dependency on water usage and low requirement for waste treatment, and also the possibility of regenerating the sorbent used in the process. The potential regeneration of the sorbent used in dry FGD process will result in significant cost reduction while simultaneously allowing generation of highly saleable and marketable SO_2 in the form of sulfuric acid, elemental sulfur or liquid SO_2. One of the most important aspects of dry regenerative FGD is that the majority of the sorbents are naturally available, can be easily synthesized or made from wastes of other processes, making the method economically viable [1].

Various types of porous sorbents have been developed for the removal of SO_2 from flue gas such as activated carbons, zeolites, metal oxides and mesoporous silica [2–5]. The utilization of mesoporous silica such as MCM-41, SBA-15 and KIT-6 are highly attractive due to their high specific surface areas, ordered pore structures and variety of morphologies. The ordered structure provides an excellent space for introduction of various additives, e.g., metal salts or amine-based additives that improve their capacity in adsorbing SO_2 available in flue gas [6]. KCC-1 is another type of mesoporous silica which has been reported to be superior to the earlier ones due to its unprecedented high surface area

✉ Naimah Ibrahim
naimah@unimap.edu.my

1 Faculty of Civil Engineering Technology, Universiti Malaysia Perlis, 02600 Arau, Perlis, Malaysia

2 Faculty of Chemical Engineering Technology, Universiti Malaysia Perlis, 02600 Arau, Perlis, Malaysia

3 School of Chemical and Energy Engineering, Faculty of Engineering, Universiti Teknologi Malaysia, UTM Johor Bahru, 81310 Skudai, Johor, Malaysia

and good thermal, mechanical and hydrothermal properties. Recently, the use of fibrous mesoporous silica KCC-1 has been reported in gas cleaning especially for carbon dioxide [7, 8], however, its use in the removal of SO_2 is still lacking. Additionally, the use of basic additives such as metal oxides is important to counter the increase in acidity brought by the adsorbed SO_2. In our preliminary work [9], the performance of KCC-1 was enhanced by modification with alkaline metal and alkaline earth metal, sodium and calcium respectively, with greater adsorption capacity exhibited by the latter. The properties of calcium-modified KCC-1 prepared at different metal loading, calcination temperature and calcination time and its removal capacity was further discussed in an optimization study of the system [10].

From an industrial point of view, two parameters are necessary for an adsorbent to be employed: (i) high removal capacity and (ii) rapid adsorption rate [11]. Due to this reason, knowledge of the kinetics, thermodynamics and mass transfer mechanism of the adsorption process is an important aspect to be understood. The experimental results are usually fitted with adsorption kinetic models to determine the reaction mechanism between the adsorbate and the sorbent and evaluate the influence of operating and design parameters [12]. Due to the nature of breakthrough experiments which require continuous measurement, a non-linearized model usually works better in representing the experimental data. Pseudo-first order, pseudo-second order and Avrami are among kinetic models which can be used in describing the gaseous adsorption kinetics and the relationship between the adsorbate and adsorbent [13]. Various literatures have reported fitting of SO_2 adsorption experimental data commonly with pseudo-first order and pseudo-second order kinetic models [14–17]. Nonetheless, most of these adsorption processes were determined to undergo both physisorption and chemisorption, suggesting that the Avrami kinetic model may be a better fit. To our best knowledge, the validity of Avrami kinetic models are yet to be confirmed in SO_2 adsorption studies but multiple studies regarding adsorption of CO, CO_2 and NO have proven its suitability in explaining the adsorption kinetics [18–20]. SO_2 adsorption is mutually reported by various studies to be exothermic, implying that the process is governed by reaction temperature negatively. In the context of isotherm studies, SO_2 adsorption may follow either Freundlich or Langmuir isotherm model of the two most commonly studied models, but the latter may only be suitable at low concentration [21]. Similar to other adsorption processes, the mass transfer process of SO_2 molecules may be controlled by either film diffusion, intraparticle diffusion or combination of both.

The purpose of this study is to understand the removal of SO_2 gas by KCC-1 mesoporous silica modified with calcium salts by analyzing the kinetics, thermodynamics, isotherm and mass transfer mechanism of the adsorption process. The performance of the modified KCC-1 was studied in a laboratory scale fixed bed reactor where two reaction parameters: reaction temperature and inlet SO_2 concentration were varied. The experimental data of adsorption at different reaction temperatures were then fitted with pseudo-first order, pseudo-second order and Avrami kinetic models to determine their applicability, especially for the latter. The results were also used in determining thermodynamic parameters of the reaction and in analyzing the mass transfer mechanism of SO_2 adsorption. Additionally, the adsorption isotherm behavior was analyzed based on the results from adsorption with different SO_2 concentrations.

2 Experimental

2.1 Materials

KCC-1 mesoporous silica was synthesized via microwave-assisted hydrothermal method as follows: (i) Mixture A was prepared by dissolving tetraethyl orthosilicate (TEOS) in a solution of cyclohexane and 1-pentanol with ratio of 1:23.08:1.08, respectively; and stirred in a Teflon bottle; (ii) Mixture B was made by mixing cetylpyridinium bromide (CTAB) and urea (0.22:0.83) in distilled water and the resultant solution was added to mixture A; (iii) The mixture of obtained were stirred at 298 K for 30 min and subsequently subjected to intermittent MW irradiation of 400 W for 4 h; (iv) The product obtained was cooled, centrifuged, and rinsed before dried overnight at 383 K and later calcined for 6 h at 823 K. All molar ratios used for solution mixture preparation was determined based on preliminary optimization studies which results in production of mesoporous silica with superior properties. All chemicals used were obtained from QRec, Malaysia.

Calcium metal was introduced onto KCC-1 via wet impregnation method as already described in our previous work [9] using calcium nitrate tetrahydrate ($Ca(NO_3)_2 \cdot H_2O$) obtained from Sigma-Aldrich (99 + %, ACS Reagent). KCC-1 was added to the calcium nitrate solution of 5 wt. % metal loading and stirred continuously for 2 h at room temperature. The mixture was then double-boiled at 343 K and the resultant was oven-fried overnight at 383 K and calcined for 6.5 h at 923 K with a heating rate of 3 K/min. These modification parameters were determined based on preliminary studies.

2.2 Characterization of samples

Surface morphology of the Ca-modified KCC-1 mesoporous silica was determined using JEOL JSM-7600F field emission scanning electron microscope (FESEM) using secondary electron image (SEI) signal at magnification of ×20,000.

The samples were coated with platinum coating prior to characterization to improve the sample imaging. Surface area and porosity of the samples were characterized using nitrogen (N_2) adsorption–desorption (Tristar 3000) at 77.35 K, while the samples were degassed at 393 K for 3 h. The surface area and pore size were determined via Brunauer–Emmett–Teller (BET) analysis and Barrett-Joyner-Halenda (BJH) model, respectively. The crystalline structure of the sample was examined by X-ray diffraction (XRD) with Bruker D2 Phaser X-ray powder diffractometer (Cu Kα radiation, 30 kV, 10 mA) at a scan range of $2\theta = 5$–$90°$ with a scan rate of 0.1 s/step. The crystallinity was calculated using Scherrer equation, as in Eq. 1 [9]:

$$L = \frac{K\lambda}{FWHM \cos\theta} \tag{1}$$

where L = crystallinity of sample, K = Scherrer constant (0.94), λ = ray wavelength (Cu Kα = 0.15418 nm), FWHM = full width at half maximum of peak and θ = diffraction angle of peak.

2.3 SO$_2$ adsorption experiments

SO$_2$ adsorption performance of Ca-modified KCC-1 (Ca/KCC-1) was examined via a breakthrough adsorption experiment. In a typical breakthrough experiment, 0.3 g of Ca/KCC-1 (average sorbent bed = 0.8 cm) was packed in the middle of a vertical quartz tube (OD = 12.7 mm, ID = 8.8 mm) with quartz wool and placed inside a tubular furnace installed with programmable controller. The void spaces were filled with quartz wool. A special mixed gas of 0.3% SO_2/N_2 (Linde Singapore) was utilized as synthetic industrial flue gas in this study. The schematic diagram of the experimental setup is shown in Fig. 1. Prior to the sorption stage, the adsorbent bed was degassed with pure

nitrogen at 423 K for 60 min to eradicate any impurities. The reactor was then cooled to the desired adsorption temperature. The adsorption study was conducted by passing through the Ca/KCC-1 adsorbent bed a stream of SO_2 gas (200 mL/min), while the outlet stream was measured continuously for 2 h using Testo 340 analyzer. The flow rate was selected to emulate gas hourly space velocity (GHSV) of 25,000 h^{-1} which is typical value for exhaust gas condition [22].

The adsorbent bed was considered to have achieved breakthrough once the gas analyzer detected the presence of 5% of inlet SO_2 concentration in the outlet stream. Due to the different performance of each sample after 2 h of experiment and for fair comparison purposes, the adsorption capacity was calculated at $C/C_0 = 0.8$ using adsorption capacity equation as shown in Eq. 2, where C_0 and $C_A = SO_2$ inlet concentration and SO_2 concentration at specific time (mg/L), Q_f = gas flow rate (L/min), y_t = gas molar fraction and m_c = mass of adsorbent bed (g) [23].

$$q = \frac{C_0 Q_f y_t}{m_c} \int_0^\infty \left(1 - \frac{C_A}{C_0}\right) dt \tag{2}$$

2.4 Studies on adsorption kinetics, thermodynamics, isotherm and mass transfer mechanism

Adsorption studies were conducted at different reaction temperatures (313–393 K) and inlet SO_2 concentrations (1500–2500 ppm) to further understand the process of SO_2 removal by Ca/KCC-1 in terms of adsorption kinetics, thermodynamics, isotherm and mass transfer mechanism. The reaction temperature was chosen based on the exothermic

Fig. 1 Schematic diagram of SO$_2$ breakthrough experiment setup
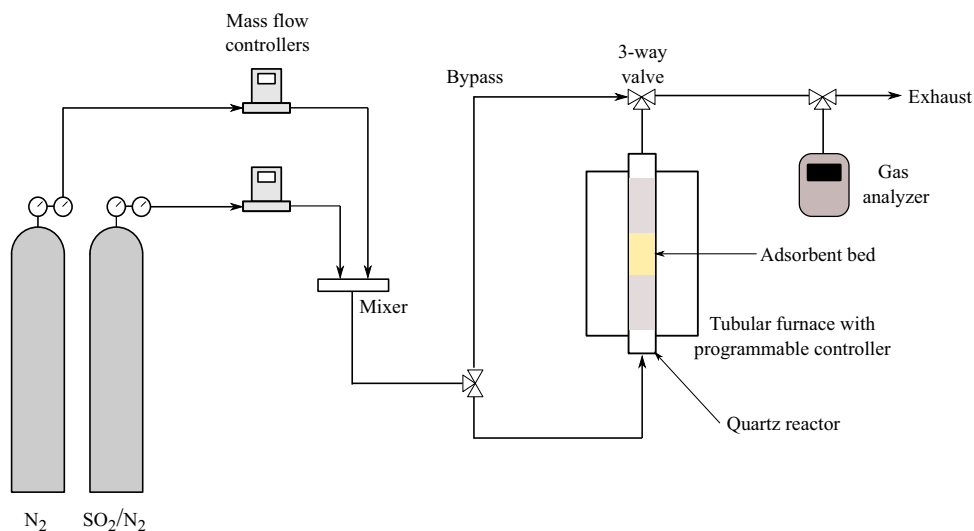
nature of the process and limitation of equipment utilized in this study. The range of SO_2 concentration was selected based on the typical concentration of SO_2 (1800 ppm) emitted in flue gas from combustion of medium to high sulfur-content fossil fuels [24]. The experimental parameters and adsorption models studied are summarized in Fig. 2.

2.4.1 Adsorption kinetics

The experimental results from adsorption studies with varying reaction temperatures were fitted with three non-linearized kinetic models, pseudo-first order, pseudo-second order and Avrami due to their simplicity in describing the gaseous adsorption kinetics and the relationship between the adsorbate and adsorbent. The two commonly utilized kinetic models; pseudo-first order and pseudo-second order assume that adsorption occurs on localized sites, there is no interaction between the adsorbed molecules, and adsorption energy is independent of the sorbent surface coverage at constant concentration of adsorbate [25]. The difference between these two models is that the molecules uptake by the sorbent is governed by a first-order rate equation for the former and a second-order rate equation for the latter. Non-linearized equations of these two models are shown in Eqs. 3 and 4, respectively.

$$q_t = q_e\left(1 - e^{-k_1 t}\right) \tag{3}$$

$$q_t = \frac{k_2 q_e^2 t}{1 + k_2 q_e t} \tag{4}$$

where q_t and q_e = amount of adsorbate adsorbed per unit mass of sorbent (mg/g) at time t, and at equilibrium, respectively, k_1 = pseudo-first order rate constant (min^{-1}) and k_2 = pseudo-second order rate constant (g/mg•min).

On the other hand, Avrami kinetic model assumes a simultaneous occurrence of multiple adsorption pathways of physical and chemical adsorption [26, 27]. The non-linearized equation for this model is shown in Eq. 5, where k_a = Avrami rate constant (min^{-1}) and n = Avrami exponent. Avrami exponent is typically in fractional form and presents the possible mechanism change in the process. The value of n shows the dimension of the growth of the adsorbed species on the active sites present on the sorbent where n = 2 and 3 represent one-dimensional and two-dimensional growth, respectively [26]. The value of k_a is an overall constant which exhibits the presence of various reaction steps [28].

$$q_t = q_e\left(1 - e^{(-k_a t)^n}\right) \tag{5}$$

2.4.2 Adsorption thermodynamics

The experimental data of adsorption studies conducted at different reaction temperatures were further utilized to determine the thermodynamic parameters of the adsorption process. Activation energy (E_a) which represents the minimum amount of energy required to overcome the minimum barrier energy of a particular reaction was calculated using Arrhenius equation, shown in Eq. 6, where k = rate constant, R = universal gas constant and T = temperature (K).

$$\ln k = \ln A - \frac{E_a}{RT} \tag{6}$$

The enthalpy ($\Delta H°$) and entropy ($\Delta S°$) of the adsorption process was obtained from the slope and the intercept of van 't Hoff equation (Eq. 7) where K_D = distribution coefficient and Ce = adsorbate concentration on the sorbent at equilibrium. A positive or negative value of $\Delta H°$ demonstrates that the adsorption process is exothermic or endothermic in nature, respectively. A negative $\Delta S°$ suggests

Fig. 2 Summary of experimental parameters and models used

Adsorbent	Fixed reaction parameters	Variable reaction parameters	Model used
Calcium-modified KCC-1	Flow rate: 200 ml/min Adsorbent dosage: 0.3 g	Reaction temperature: 313 - 393 K SO$_2$ inlet concentration: 1500 ppm	Kinetics: Pseudo first order, pseudo second order, Avrami Thermodynamics: Arrhenius, van 't Hoff equation Mass transfer mechanism: Intraparticle diffusion, Boyd film diffusion model
		Reaction temperature: 313 K SO$_2$ inlet concentration: 1500 - 2500 ppm	Isotherm: Freundlich, Langmuir

that the solid–gas interface changes from random stage to ordered stage during adsorption process with lower degree of freedom of the adsorbates, and vice versa for positive $\Delta S°$ [1, 29].

$$\ln K_D = \ln \frac{q_e}{C_e} = \frac{\Delta S°}{R} - \frac{\Delta H°}{RT} \qquad (7)$$

The degree of spontaneity of the adsorption process at a particular temperature can be determined using Gibbs free energy ($\Delta G°$) as in Eq. 8. Negative $\Delta G°$ demonstrates that the adsorption process is spontaneous and favorable while positive $\Delta G°$ indicates that the process occurs in a non-spontaneous manner. Small value of $\Delta G°$ suggests that the adsorption process is controlled by diffusion process rather than chemical reaction [30].

$$\Delta G° = \Delta H° - T\Delta S° \qquad (8)$$

2.4.3 Adsorption isotherms

Results obtained from adsorption studies conducted with different inlet SO_2 concentrations were fitted with Freundlich and Langmuir isotherm models to determine the nature of SO_2 adsorption onto the solid adsorbent under equilibrium conditions at constant temperature. Freundlich isotherm represented by Eq. 9 where K_F = adsorption capacity (L/mg) and $1/n$ = adsorption intensity, assumes a heterogeneous surface properties with multilayer adsorption and exponential distribution of the active sites on the sorbent and their energies [31].

$$\log q_e = \log K_F + \frac{1}{n} \log C_e \qquad (9)$$

Langmuir isotherm model assumes that formation of monolayer adsorbate occurs on the surface of the adsorbent and no further adsorption takes place once the active sites are fully occupied [32]. This model considers the surface coverage by balancing the equilibrium of adsorption–desorption rates [31]. Adsorption and desorption are proportional to the fraction of the sorbent surface available and covered, respectively. The linearized form of Langmuir model is shown in Eq. 10, where Langmuir constant, K_L is related to adsorption capacity (mg/g), correlating with the surface area and porosity of the sorbent and Q_0 is the amount of adsorbate adsorbed at saturation (mg/g).

$$\frac{C_e}{q_e} = \frac{1}{K_L} + \frac{C_e}{Q_0} \qquad (10)$$

2.4.4 Mass transfer mechanism

Heterogeneous adsorption of gaseous molecules on solid adsorbent typically comprises bulk diffusion, film diffusion, inter-particle diffusion, surface diffusion and intra-particle diffusion. Mass transfer mechanism of the adsorption process may be determined by distinguishing the rate limiting step of the process. Majority of gas adsorption is critically governed by either intra-particle diffusion, film diffusion or both [33, 34]. Intra-particle diffusion (IPD) model assumes that the external mass transfer is only significant at the beginning of the process, constant pore diffusivity and radial diffusion of the gas adsorbate [35]. The equation representing this model is shown in Eq. 11 where q_t = amount of adsorbate adsorbed per unit mass of sorbent (mg/g) at time, t, k_{id} = IPD rate constant ((g•min$^{-0.5}$)/mg) and C = initial adsorption (mg/g) [36]. A linear plot signifies that an adsorption process is controlled by IPD, where in the case that the plot passes through the origin, IPD is the sole rate limiting step. Nonetheless, the plot of this model is rarely a single linear plot and is commonly a multi-linear plot, each representing a different stage of the adsorption process [11].

$$q_t = k_{id}t^{0.5} + C \qquad (11)$$

Boyd's film diffusion model takes into account the effect of external mass transfer resistance during the diffusion of gas adsorbate through the gas film. This step limits the adsorption stage mainly due to the gas film surrounding the adsorbent particles [11]. The effect of film diffusion is determined by plotting Bt against time, where Bt is calculated as follows:

$$F = \frac{q_t}{q_e} \qquad (12)$$

$$\text{For } F > 0.85 \quad Bt = -0.4977 - \ln(1 - F) \qquad (13)$$

$$\text{For } F < 0.85 \quad Bt = \left(\sqrt{\pi} - \sqrt{\pi - \frac{\pi^2 F}{3}} \right)^2 \qquad (14)$$

Similar to the IPD model, a linear plot passing through the origin signifies that the adsorption process is solely limited by the film diffusion step. A linear plot without passing the axes origin or a non-linear plot indicates that the rate limiting step of the process is film diffusion or combination of both film and intra-particle diffusion.
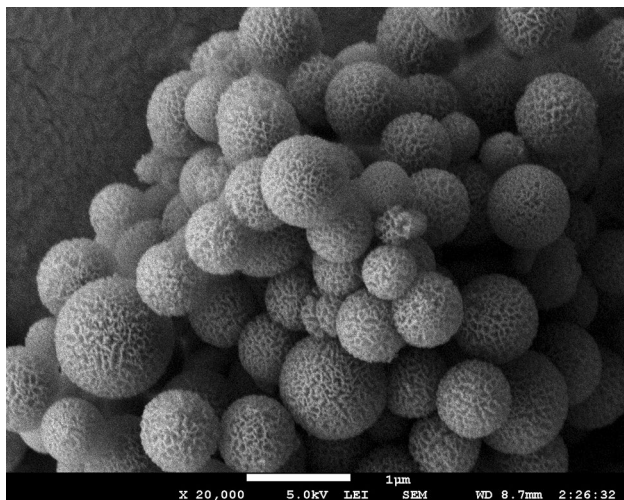
Fig. 3 FESEM micrograph of calcium-modified mesoporous silica (Ca/KCC-1)

3 Results and discussion

3.1 Sample characterization

Calcium-modified KCC-1 mesoporous silica demonstrates a well-defined fibrous morphology of dendrimeric silica fibers shown in Fig. 3. The presence of these dendrimeric fibers on KCC-1 results in highly accessible surface area and active sites [37]. Several broken spheres observed in Fig. 3 are attributed to the agglomeration of calcium metal which slightly distorts the structure of KCC-1 mesoporous silica framework.

The introduction of calcium metal on KCC-1 has been optimized for this work, but no significant changes can be observed on N_2 adsorption–desorption isotherm and X-ray diffractograms of the samples compared to the samples used in our previous study [9, 10]. Since the only identified differences between the samples are the intensity of N_2 adsorption–desorption and the full width at half maximum (FWHM) of the XRD peaks, both plots are not included in this manuscript. Similar to the previous work, Ca/KCC-1 sample in this work demonstrates a Type IV(a) isotherm with H3 hysteresis between $P/P_0 = 0.5–1.0$, representing mesoporous materials with characteristics of capillary condensation and non-uniform slit-shaped pores [38]. The highest N_2 uptake by the sample is 2723.22 cm^3/g. Similarly the X-ray diffractogram of the sample used in this work also indicates the presence of isolated CaO on the surface of KCC-1 [39], albeit the peaks are poorly defined due to the amorphous nature of the sample. The peak search function has been strictly restricted on finding SiO_2 and CaO only where good agreement between experimental data and standard diffraction angle

Table 1 Properties of Ca-modified mesoporous silica KCC-1

Surface area (m^2/g)	Total pore volume (cm^3/g)	Average pore size (nm)	Detected phase	CaO crystallite size (nm)	Crystallite structure
1089.84	3.09	11.3	Calcium oxide	74.39	Cubic

based on JCPDS powder diffraction card is attained. The analysis shows peaks corresponding to amorphous SiO_2 at $2\theta = 15–30°$, with maximum at 22° based on JCPDS Card No 00-041-1485 [40] and calcium oxide at $2\theta = 32.20°$ (111), 37.32° (200), 53.90° (220), 64.16° (311), 67.37° (222) and 79.53° (400) based on JCPDS Card No 82-1691 [41]. Detailed properties of Ca-modified KCC-1 are summarized in Table 1.

3.2 SO$_2$ adsorption at different reaction temperature

Figure 4 shows the breakthrough curves of SO_2 adsorption by Ca/KCC-1 conducted at different reaction temperatures between 313 and 393 K. The results exhibit strong dependency of SO_2 adsorption on reaction temperature implying that the reaction is thermodynamically controlled. In this study, the performance of Ca/KCC-1 is significantly worsened with increasing temperature. The experimental details of each run are summarized in Table 2.

The highest removal was obtained at 313 K where the adsorbent bed is considered to have achieved breakthrough after 201 s at an adsorption capacity of 3241.94 mg/g. As the reaction temperature increases, a shorter breakthrough
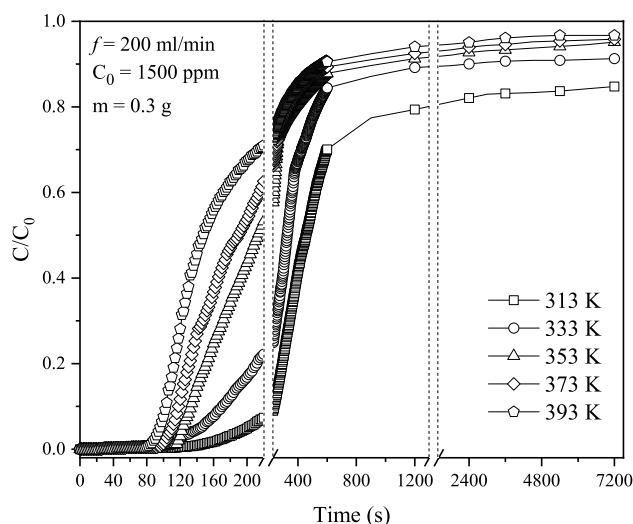

Fig. 4 Breakthrough curves of SO_2 adsorption on Ca/KCC-1 at different reaction temperatures

Table 2 Experimental data of SO$_2$ adsorption on Ca/KCC-1 at different reaction temperatures

Reaction temperature (K)	Breakthrough time at C/C$_0$=0.05 (s)	Time at calculated adsorption capacity C/C$_0$=0.8 (s)	Adsorption capacity at C/C$_0$=0.8 (mg/g)
313	201	1800	3241.94
333	144	532	1768.22
353	123	380	834.78
373	111	353	673.61
393	96	308	471.94

time and significant reduction in adsorption performance can be observed. The performance at 393 K is 6.8 times smaller compared to the finding at 313 K. Similar results have been observed by other researchers using various sorbents e.g., activated carbon, MCM-41, where superior adsorption performance was obtained at lower temperature [36, 42]. Nonetheless, the adsorption capacities obtained at all 5 temperatures tested in this work are higher compared to the previously reported mesoporous silica e.g., MCM-41, SBA-15, KIT-5, with adsorption capacities between 39.71 and 299.80 mg SO$_2$/g sorbent. The superior performance by modified KCC-1 is conceivably due to its unprecedented high surface area and the sufficient basicity provided by calcium metal which counters the increase in acidity associated with adsorbed SO$_2$. However, it should be emphasized that this significant discrepancy may also be affected by the operational reaction conditions utilized in the studies.

Conducting the adsorption process at a temperature lower than 313 K may be beneficial but not conducted in this study due to instrument limitation. The decrease in adsorption performance at higher reaction temperatures may be attributed to the exothermic nature of the process which favors lower temperature. The adverse effect at higher temperature may be contributed by (i) reduction of enthalpy due to lower free energy and degree of freedom during the process and (ii) low heat of adsorption due to surface heterogeneity [43].

3.3 Adsorption kinetics

The non-linear fit of SO$_2$ adsorption data onto Ca/KCC-1 conducted at different reaction temperatures (at constant
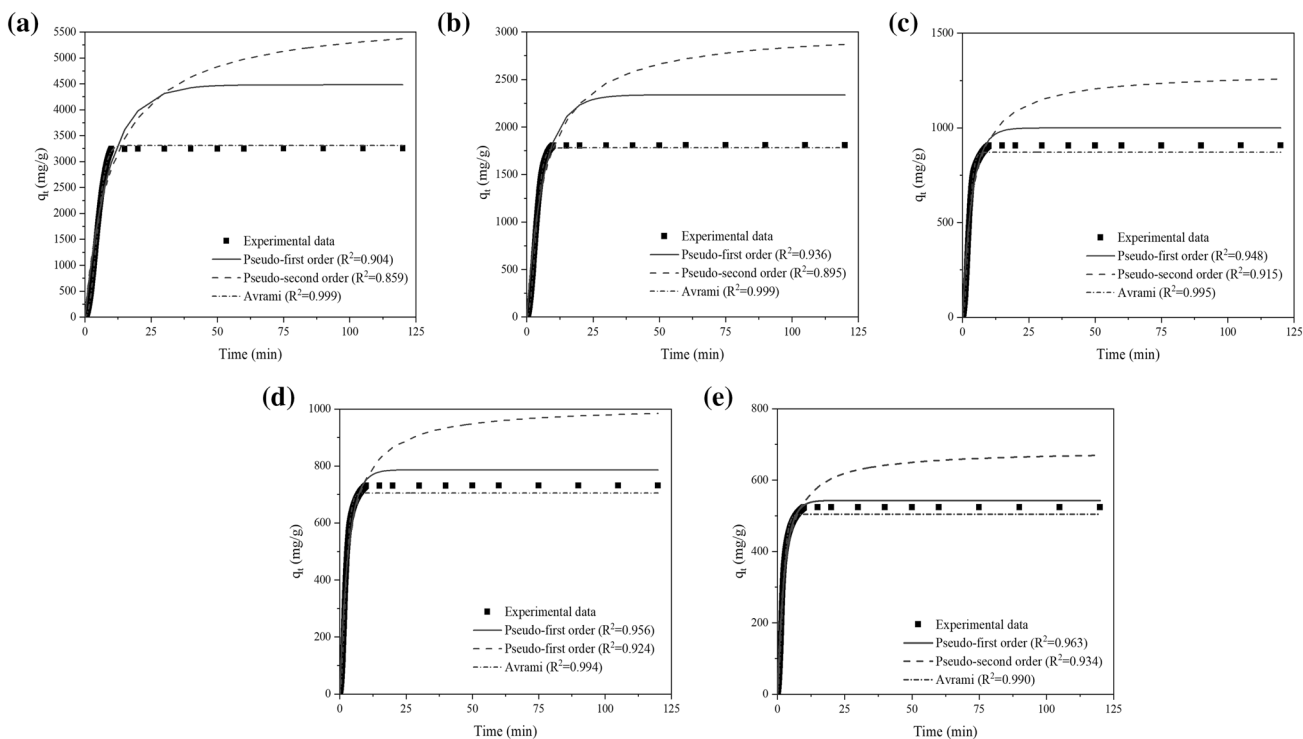

Fig. 5 Non-linear fit of pseudo-first order, pseudo-second order and Avrami kinetic model for SO$_2$ adsorption at **a** 313 K, **b** 333 K, **c** 353 K, **d** 373 K and **e** 393 K

Table 3 Kinetic parameters of three kinetics models fitted with adsorption data at different reaction temperature

Kinetics model	Reaction temperature (K)				
	313	333	353	373	393
Pseudo-first order					
R^2	0.9039	0.9363	0.9477	0.9561	0.9634
k_1	0.1097	0.1554	0.2769	0.3107	0.3772
Pseudo-second order					
R^2	0.8590	0.8950	0.9150	0.9244	0.9338
k_2	1.650×10^{-5}	4.665×10^{-5}	1.997×10^{-4}	2.937×10^{-4}	5.525×10^{-4}
Avrami					
R^2	0.9999	0.9997	0.9952	0.9944	0.9901
k_a	0.1781	0.2387	0.3524	0.3770	0.4310
n	2.134	2.056	1.950	1.783	1.597

pressure and sorbent dosage) with all three kinetic models and their parameters are shown in Fig. 5 and Table 3, respectively. Apparently, the Avrami kinetic model is applicable to explain the adsorption process within the range of reaction temperature tested, with correlation coefficient, $R^2 > 0.99$ for all temperatures. This suggests that adsorption of SO_2 onto Ca/KCC-1 is a multi-linear process where both physisorption and chemisorption contribute to the adsorption process [18]. The value of Avrami exponent, n, between 1.6 to 2.1 signifies a one-dimensional growth of SO_2 adsorbed molecules on the available active sites on the surface of Ca/KCC-1 [26], while the value of $n > 1$ implies that there is coexistence of different SO_2 adsorption mechanisms (physisorption and chemisorption) and the adsorption follows multiple kinetic orders that change during the contact of SO_2 with the adsorbent [11, 26, 28]. This also implies that the initial formation of adsorption sites is presumably uniform on the adsorbent surface and subsequent adsorption may have occurred near the existing adsorption sites, resulting in alteration of adsorption sites uniformity [26]. The reduction of Avrami exponent upon increase in temperature from 313 to 393 K indicates that the adsorption process becomes less predominated by diffusional processes, the coexistence of different mechanisms decreases, and the adsorption process is less dependent on contact time at higher temperature [11, 13]. The rate of adsorption increases with increasing reaction temperature which explains the shorter time required for the SO_2 molecules to achieve sorbent breakthrough. This can be attributed to the effective diffusivity coefficient ($D_e = D/R^2$) of the process. Upon increment of reaction temperature, thermal velocities of the SO_2 molecules will increase and this ultimately results in faster diffusion of SO_2 molecules onto the active sites on the sorbent. On the other hand, pseudo-first order and pseudo-second order models do not fit well with the experimental data compared to Avrami model and are not further discussed.

As discussed previously, the majority of the literature studying SO_2 adsorption did not consider the applicability

of the Avrami kinetic model. The results of this study prove that the Avrami kinetic model is better in explaining a reaction where multiple reaction pathways may take place during the process. It should also be noted that increasing the reaction temperature slightly decreases the R^2 values observed in Avrami model plot, while the R^2 values of the other two models increase significantly. It is safe to assume that the other two models may be more suitable to explain the adsorption process at reaction temperatures higher than 393 K, nonetheless, the SO_2 adsorption capacity may suffer greatly at such temperatures.

3.4 Adsorption thermodynamics

Thermodynamic parameters for the adsorption process were studied to prove several hypotheses discussed in the previous section. The Arrhenius plot for the calculation of activation energy and van 't Hoff plot for the calculation of enthalpy and entropy of reaction are shown in Fig. 6. The thermodynamic parameters calculated from these plots are summarized in Table 4.

As can be seen in Fig. 6, the experimental results can be distinguished into two distinct regions based on reaction temperature: Region 1 (313–353 K) and Region 2 (353–393 K). The activation energy of the process decreases from 15.61 to 5.77 kJ/mol from Region 1 to Region 2, implying that the reaction at higher temperature is faster due to the lower activation energy requirement. As discussed before, this is indeed true as the rate of reaction of the adsorption process is significantly faster as the reaction temperature increases. The activation energy of the whole process is within the range of activation energies (1.5–29 kJ/mol) reported by various related studies [12, 44]. As the activation energy is lower than 20 kJ/mol, the majority of the SO_2 molecules is conceivably adsorbed on Ca/KCC-1 via physisorption [45]. Low activation energy at higher temperature also implies that the strength of adsorption increases. This
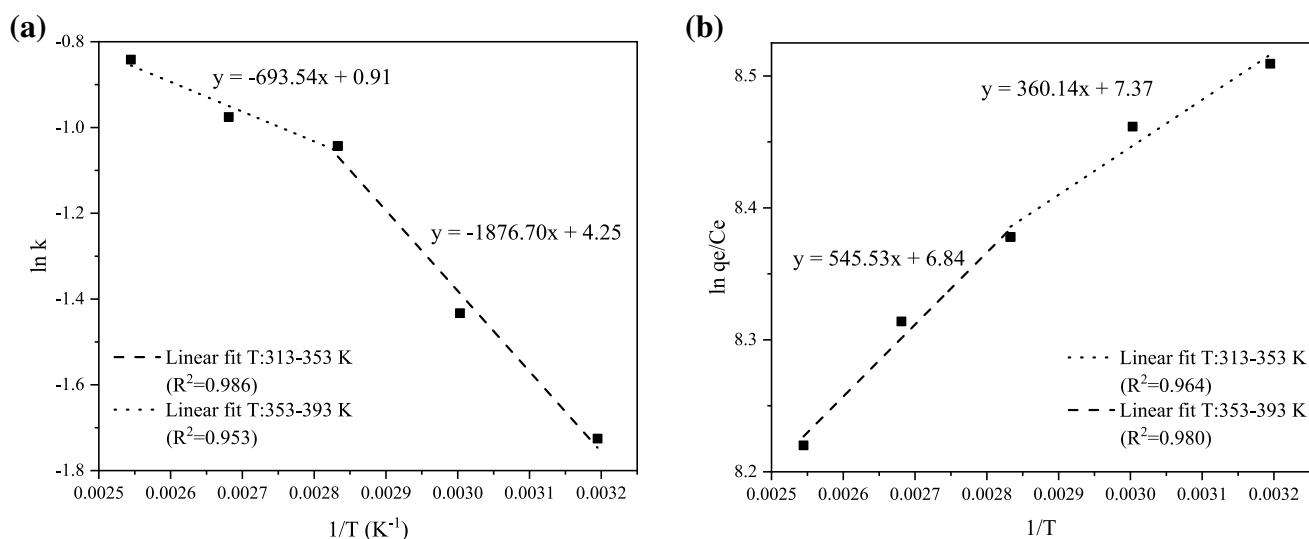
Fig. 6 Plots of **a** Arrhenius and **b** van 't Hoff equation for the calculation of thermodynamics parameters

Table 4 Thermodynamic parameters of SO$_2$ adsorption on Ca/KCC-1

Parameters	Region 1 (313–353 K)	Region 2 (353–393 K)
Activation energy, Ea (kJ/mol)	15.61	5.770
Arrhenius pre-exponential factor, A	70.03	2.480
Enthalpy, ΔH (J/mol)	− 2994	− 4536
Entropy, ΔS (J/mol•K)	61.24	56.86

Table 5 Gibbs free energy of SO$_2$ adsorption at different reaction temperature

Reaction temperature (K)	Gibbs free energy, ΔG (kJ)
313	− 22.19
333	− 23.38
353	− 24.56
373	− 25.74
393	− 26.93

supports the findings from the kinetic study where the coexistence of different mechanisms (physisorption and chemisorption) reduces to a lesser extent at higher temperature. The Arrhenius pre-exponential factor, A, describes the fraction of SO$_2$ molecules with an energy higher or equal to the activation energy, resulting in successful collision with Ca/KCC-1 [13]. The value of A significantly worsens beyond 353 K even though the value of activation energy is much lower. This result implies that fewer amounts of SO$_2$ molecules are able to collide with the adsorbent, subsequently leading to poor SO$_2$ adsorption performance.

It can be assumed that the poor performance of Ca/KCC-1 in adsorbing SO$_2$ at higher reaction temperature is indebted to the exothermic nature of the process and the reduction of enthalpy as the adsorption occurs. These hypotheses are proven as the adsorption process at all reaction temperatures are exothermic and the adsorption enthalpy significantly decreases with increasing reaction temperature from -2994 to -4535 J/mol. The entropy of the adsorption process is positive for both regions, demonstrating high sorbent affinity towards SO$_2$ and that the adsorption process goes from an ordered stage on the surface of

KCC-1 towards an increasingly random stage with higher degrees of freedom [1, 46]. A slight reduction in the value of entropy from Region 1 to Region 2 is contributed by lesser degrees of freedom for SO$_2$ to be adsorbed on KCC-1 at higher temperature, consequently resulting in lower adsorption capacity [47].

Gibbs free energy (ΔG) is a parameter utilized in determining the degree of spontaneity of a specific process at a given temperature. The adsorption of SO$_2$ onto Ca/KCC-1 is spontaneous and favorable as the total free energy is negative (ΔG < 0) at all temperatures, as shown in Table 5. Small ΔG values also suggest that the process is restricted by diffusion rather than a chemical reaction [30]. The value of ΔG which decreases with an increase in temperature on the other hand implies that the adsorption process is highly feasible at higher temperature [45]. This clearly supports the findings from the kinetic study, which showed that the rate of reaction is significantly enhanced upon increase in temperature conceivably due to the ease of SO$_2$ molecules to diffuse through the stagnant film and into the pores.

Table 6 Experimental data of SO_2 adsorption on Ca/KCC-1 at different inlet SO_2 concentration

Inlet SO_2 concentration (ppm)	Breakthrough time at $C/C_0 = 0.05$ (s)	Time at calculated adsorption capacity $C/C_0 = 0.8$ (s)	Adsorption capacity at $C/C_0 = 0.8$ (mg/g)
1500	201	1800	3242
1750	159	365	1529
2000	87	238	519.4
2250	74	215	474.8
2500	51	178	327.9

3.5 SO_2 adsorption with different inlet SO_2 concentration

Figure 7 shows the SO_2 breakthrough curves obtained with different inlet SO_2 concentrations (1500 – 2500 ppm), while the experimental details of each run are summarized in Table 6. In general, the performance of SO_2 removal by Ca/KCC-1 differs significantly with the variation of SO_2 concentrations. Highest adsorption capacity is achieved at the lowest concentration of SO_2 (1500 ppm) and the adsorption performance significantly decreases with increasing concentrations. The SO_2 adsorption capacity decreases by more than half upon increasing the SO_2 concentration from 1500 to 1750 ppm and is reduced by 10 times at SO_2 concentration of 2500 ppm. Similar results were reported in the SO_2 removal by bacterial residue-based activated carbon [48], TiO_2 [49], ceramic membrane contactor [50] and MnO_2/γ-Al_2O_3 [51]. Nonetheless, similar to the results obtained by varying the reaction temperature, the performance of calcium-modified KCC-1 in removing SO_2 at all five different concentrations tested is still higher than the other mesoporous silica reported in the literature.
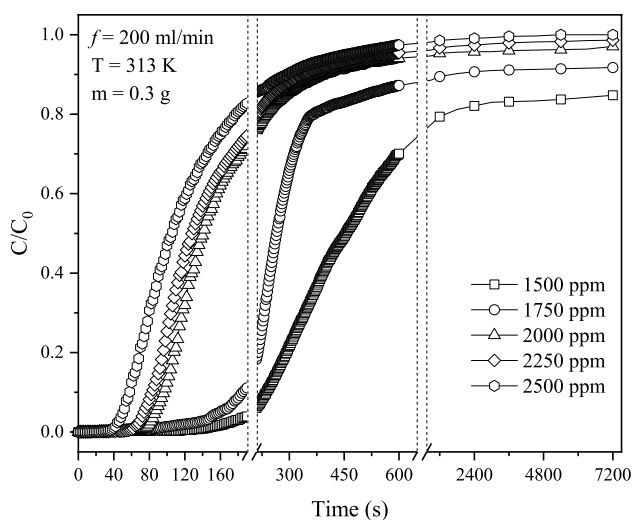
Fig. 7 Breakthrough curves of SO_2 adsorption onto Ca/KCC-1 at different inlet SO_2 concentrations

In theory, higher inlet SO_2 concentration is highly beneficial as more collisions occur between the gas adsorbates, leading to higher partial pressure and consequently resulting in better driving force for diffusion of SO_2 molecules towards the active sites available on the Ca/KCC-1. However, the amount of adsorbent used is equally important due to the synergistic effect between these two factors in adsorption studies. With the same amount of adsorbent used, the number of active sites available in all cases are similar. In such cases, an increase in the amount of SO_2 molecules does not only bring higher diffusional driving force, culminating in a faster rate of adsorption [52], but also contributes to quick saturation of the Ca/KCC-1. Apparently this phenomenon leads to faster breakthrough time and results in poor adsorption capacity [53].

3.6 Isotherm studies

The experimental data from Sect. 3.5 are fitted with Freundlich and Langmuir isotherm models to study the interaction between SO_2 adsorbates and the surface sites of Ca/KCC-1 sorbent. The linear plots of both models are shown in Fig. 8, while the parameters for each model are summarized in Table 7, calculated based on the slope and the intercept of the linear plots.

The experimental data clearly fit better with the Freundlich isotherm model with R^2 value of 0.984 compared to the poorly fitted Langmuir isotherm model. This suggests that the SO_2 adsorption on Ca/KCC-1 is a multilayer adsorption on a heterogenous surface with an exponential distribution of active sites and heat of adsorption [31]. Better fit with Freundlich isotherm model can already be expected based on the result obtained from kinetic study that suggests a non-uniform adsorption trend which coincides with the characteristics of Freundlich model. In contrast to other studies, it is found that Freundlich isotherm model is appropriate to describe the adsorption processes at various inlet SO_2 concentrations, while Langmuir isotherm model is only applicable for low SO_2 concentration [21].

Of particular importance is the parameter 1/n representing the strength of the adsorption and heterogeneity obtained from the slope of Freundlich isotherm linear fit. The value
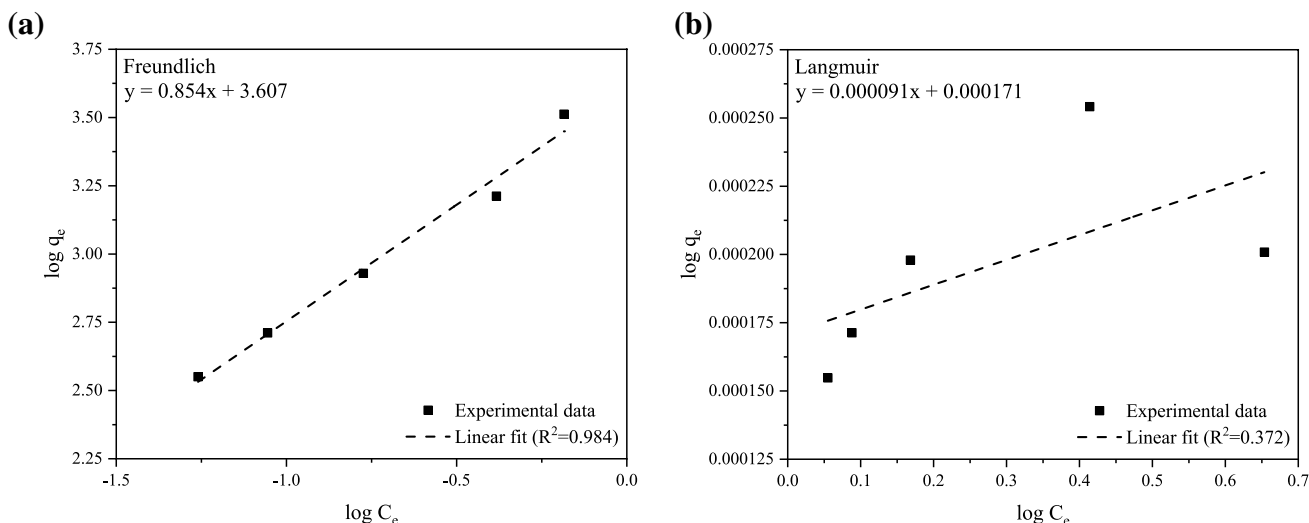
(a)

(b)

Fig. 8 Linear fits of **a** Freundlich and **b** Langmuir isotherm model for adsorption at different inlet SO_2 concentrations

Table 7 Kinetic parameters of Freundlich and Langmuir isotherm model at different inlet SO_2 concentrations

Freundlich		Langmuir	
R^2	0.9844	R^2	0.3722
$1/n$	0.8536	q_m (mg/g)	11,000
k_F (L/mg)	4048	k_L (mg/g)	$64,424 \times 10^3$

of $1/n$ indicates the type of adsorption occurred, as follows [54–57]:

(i) $1/n = 0$: an irreversible adsorption.
(ii) $0 < 1/n < 1$: a favorable adsorption, chemisorption process, strong adsorption bond due to intermolecular attraction within adsorbent, decreasing adsorption energy at higher surface concentration.
(iii) $1/n > 1$: an unfavorable adsorption, cooperative adsorption process, weak adsorption bond between adsorbate and adsorbent, increasing adsorption energy at higher surface concentration.

The value of $1/n = 0.854$ obtained in this study suggests a favorable adsorption process which possibly follows a weak chemisorption route with exponential decrease in the heat of adsorption. A larger n value commonly indicates that an adsorption is more heterogeneous. In addition, n values of 1–2 and 2–10 represent a moderate and good adsorption capacity, respectively [54, 56]. Based on our n value of 1.172, it is safe to conceive that SO_2 adsorption on Ca/KCC-1 is slightly heterogeneous and has a moderate adsorption capacity. However, it is important to note that Freundlich isotherm is an empirical model with certain limitations
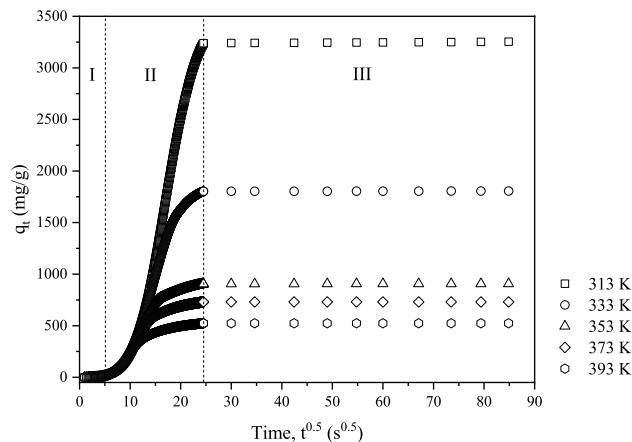

Fig. 9 IPD model plot of SO_2 adsorption at different reaction temperatures

and its linearity is only valid up to a certain concentration, above which nonlinearity can be expected.

3.7 Mass transfer mechanism

The rate limiting step of the adsorption process is determined by plotting the adsorption data with IPD model (Fig. 9) and Boyd film diffusion model (Fig. 10). The parameters for the IPD model are summarized in Table 8. IPD plots for all reaction temperatures show a multi-linear form which can be divided into three sections: (I) SO_2 diffusional mass transfer on the external surface of Ca/KCC-1, (II) gradual adsorption stage which is controlled by the intraparticle diffusion of SO_2 adsorbate on the surface and through the pores of Ca/KCC-1, and (III) final equilibrium stage with
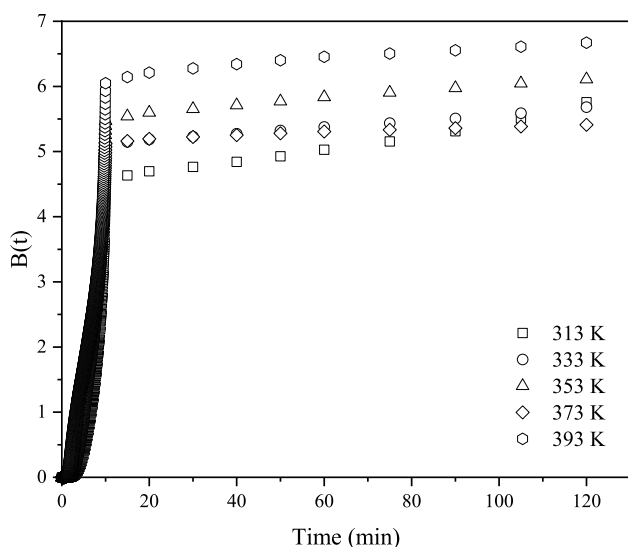
Fig. 10 Boyd film diffusion model plot of SO_2 adsorption at different reaction temperatures

Table 8 IPD parameters for SO_2 adsorption at different reaction temperatures

IPD parameters	Reaction temperature (K)				
	313	333	353	373	393
Section 1					
R^2	0.8478	0.8474	0.8474	0.8474	0.8476
$k_{id,1}$	3.898	3.902	3.902	3.902	3.900
$C_{id,1}$	− 7.778	− 7.787	− 7.787	− 7.787	− 7.784
Section 2					
R^2	0.9720	0.9630	0.8778	0.8654	0.8353
$k_{id,2}$	207.3	114.1	48.54	37.11	23.96
$C_{id,2}$	− 1752	− 760.5	− 142.7	− 67.64	9.573
Section 3					
R^2	0.9924	0.9945	0.9955	0.9869	0.9620
$k_{id,3}$	0.2282	0.04682	0.01917	0.01054	0.005223
$C_{id,3}$	3234	1802	905.2	730.1	523.2

slow adsorption process due to fewer adsorption sites available and saturation phenomenon [58].

The $k_{id,1}$ values at all temperatures are similar and much smaller compared to $k_{id,2}$ indicating that the film diffusion of SO_2 on the surface of Ca/KCC-1 is relatively slow [11]. Intraparticle diffusion of SO_2 into the mesopores starts to occur once the external surface area of Ca/KCC-1 is completely saturated. High $k_{id,2}$ indicates that the IPD stage occurs at a fast pace but this slows down significantly at higher reaction temperature. As the linear fit of Section II does not cross the axis origin, it can be concluded that the IPD stage is not the sole rate limiting step of the adsorption process [59]. On the other hand, the parameter C of the IPD

model indicates the thickness of the boundary layer where a larger C value indicates a greater effect brought by the boundary layer. Based on the negative C values for Section II at all temperatures except for 393 K, it can be inferred that the adsorption process may be controlled by the combination of film diffusion and surface adsorption [60, 61]. A negative C value also denotes that the thickness of the boundary layer significantly hinders the progress of IPD [61]. Since it is known that adsorption is a rapid process and typically not the rate limiting step, this suggests that the process is mainly limited by film diffusion and IPD.

In addition, the Boyd plots at different reaction temperatures in Fig. 10 are non-linear. Although it is safe to conclude that the film diffusion step where SO_2 molecules need to diffuse through the gas film before being adsorbed critically controls the adsorption of SO_2 onto KCC-1, the non-linearity of the plots supports the previous finding that the rate limiting step is a combination of film diffusion and intraparticle diffusion [35, 62]. Nonetheless, based on the results from IPD and Boyd models, each diffusional step appears to only limit the adsorption for a specific interval.

Based on the results obtained, the mass transfer mechanism of SO_2 adsorption on Ca-modified KCC-1 can be summarized as follows: (i) Film diffusion: mass transfer of SO_2 molecules from bulk phase through the stagnant film surrounding the particle external surface critically controls the adsorption due to the major resistance for mass transfer through the gas film; (ii) IPD: mass transfer of SO_2 from the external surface into the pores, and (iii) Adsorption process where SO_2 is attached on the surface of Ca-modified KCC-1 active sites and the process continues until equilibrium is achieved.

4 Conclusion

The applicability of calcium modified KCC-1 (Ca/KCC-1) as sorbents in dry FGD is investigated by examining the kinetics, thermodynamics, isotherm and mass transfer mechanism of the adsorption process. Reaction temperature plays a significant role in the process as high temperature is detrimental towards the ability of the sorbent to remove SO_2 due to the exothermic nature of the process and the loss of enthalpy. Increasing the inlet SO_2 concentration also significantly reduces the adsorption performance, therefore its synergistic effect with adsorbent dosage should always be considered. SO_2 molecules are adsorbed by a combination of physisorption and chemisorption as explained by Avrami kinetic model which is often overlooked in kinetic studies. Thermodynamic studies show that the process is exothermic, spontaneous and goes from ordered stage to random stage. Freundlich isotherm model can be used to describe the

adsorption process, implying that the process is a multilayer adsorption on a heterogenous surface with an exponential distribution of active sites and heat of adsorption. The mass transfer of SO_2 towards the adsorbent surface is rate limited by both film diffusion and intraparticle diffusion at the initial stage and the later stage of adsorption, respectively.

Data availability The authors confirm that the data supporting the findings of this study are available within the article.

Code availability Not applicable.

Declarations

References

1. M.M. Meimand, N. Javid, M. Malakootian, Heal. Scope **8**(2), e69158 (2019)
2. Y. Boutillara, J.L. Tombeur, G. De Weireld, P. Lodewyckx, Chem. Eng. J. **372**, 631–637 (2019)
3. N. Czuma, W. Franus, P. Baran, A. Ćwik, K. Zareska, Turkish J. Chem. **44**(1), 155–167 (2020)
4. X.M. Pham et al., J. Chem. **2019**, 2 (2019)
5. L. Wei, Z. Gao, Y. Wang, Asia-Pac. J. Chem. Eng. **12**(4), 660–670 (2017)
6. X. Huang et al., Langmuir **30**(36), 10886–10898 (2014)
7. U. Patil, A. Fihri, A.H. Emwas, V. Polshettiwar, Chem. Sci. **3**, 2224–2229 (2012)
8. M.Y.S. Hamid, S. Triwahyono, A.A. Jalil, N.W.C. Jusoh, S.M. Izan, T.A.T. Abdullah, Inorg. Chem. **57**(10), 5859–5869 (2018)
9. M. A. Hanif, N. Ibrahim, K. Md. Isa, T. A. T. Abdullah, A. A. J., Mater. Today Proc. **47**, 1323–1328 (2021)
10. M. Adli, H. Naimah, I. Khairuddin, M.I. Fahmi, M.R.T. Amran, T.A.A. Abdul, Jalil, Tailoring the properties of calcium modified fibrous mesoporous silica KCC-1 for optimized sulfur dioxide removal. Micropor. Mesopor. Mater. (2022). https://doi.org/10.1016/j.micromeso.2021.111610
11. N. Álvarez-Gutiérrez, M.V. Gil, F. Rubiera, C. Pevida, Chem. Eng. J. **307**, 249–257 (2017)
12. H. Wang, C. You, Chem. Eng. J. **350**, 268–277 (2018)
13. S. N. Kudahi, A. R. Noorpoor, N. M. Mahmoodi, J. CO_2 Util. **21**, 17–29 (2017)
14. Z. Qie et al., J. Energy Inst. **93**(2), 802–810 (2020)
15. J. Dou, Y. Zhao, X. Duan, H. Chai, L. Li, J. Yu, ACS Omega **5**, 19194–19201 (2020)
16. Z. Li et al., Chem. Eng. J. **353**, 858–866 (2018)
17. M.M. Meimand, A.J. Jafari, A. Nasiri, M. Malakootian, J. Air Pollut. Heal. **5**(2), 107–120 (2020)
18. S.I. Anthonysamy, P. Lahijani, M. Mohammadi, A.R. Mohamed, Korean J. Chem. Eng. **37**(1), 130–140 (2020)
19. N. Mozaffari, A. Mirzahosseini, N. Mozaffari, Anal. Methods Environ. Chem. J. **3**(2), 92–107 (2020)
20. C. Zhao, Y. Guo, W. Li, C. Bu, X. Wang, P. Lu, Chem. Eng. J. **312**, 50–58 (2017)
21. A. Nieto-Márquez, E. Atanes, J. Morena, F. Fernández-Martínez, J.L. Valverde, Fuel Process. Technol. **144**, 274–281 (2016)
22. P. Gaudin et al., Appl. Catal. A **504**, 110–118 (2015)
23. C.S. Lin, N. Ibrahim, N. Ahmad, M.A. Hanif, S. Abdullah, Malaysian J. Fundam. Appl. Sci. **17**(1), 84–89 (2021)
24. T.C. Drage et al., J. Mater. Chem. **22**, 2815–2823 (2012)
25. L. Largitte, R. Pasquier, Chem. Eng. Res. Des. **109**, 495–504 (2016)
26. Y. Liu, X. Yu, Appl. Energy **211**, 1080–1088 (2018)
27. S. Mutyala, M. Jonnalagadda, H. Mitta, R. Gundeboyina, Chem. Eng. Res. Des. **143**, 241–248 (2019)
28. R. Serna-Guerrero, A. Sayari, Chem. Eng. J. **161**(1–2), 182–190 (2010)
29. R.L. White, C.M. White, H. Turgut, A. Massoud, Z.R. Tian, J. Taiwan Inst. Chem. Eng. **85**, 18–28 (2018)
30. Y. Xuan, Q. Yu, H. Gao, K. Wang, W. Duan, Chem. Eng. J. **395**, 124984 (2020)
31. N. Ayawei, A.N. Ebelegi, D. Wankasi, J. Chem. **2017**, 1–11 (2017)
32. A. Dada, A. Olalekan, A. Olatunya, O. Dada, IOSR, J. Appl. Chem. **3**(1), 38–45 (2012)
33. G. Song, X. Zhu, R. Chen, Q. Liao, Y.D. Ding, L. Chen, Chem. Eng. J. **283**, 175–183 (2016)
34. H. Yu, X. Wang, C. Xu, D.L. Chen, W. Zhu, R. Krishna, Chem. Eng. J. **269**, 135–147 (2015)
35. K.O. Yoro, M.K. Amosa, P.T. Sekoai, J. Mulopo, M.O. Daramola, Int. J. Sustain. Eng. **13**(1), 54–67 (2020)
36. B. Li, C. Ma, Energy Procedia **153**, 471–477 (2018)
37. V. Polshettiwar, D. Cha, X. Zhang, J.M. Basset, Angew. Chemie **49**(50), 9652–9656 (2010)
38. M. Thommes et al., Pure Appl. Chem. **87**, 1–19 (2015)
39. S. Zhou et al., Catalysts **8**, 2 (2018)
40. C.S. Ferreira, P.L. Santos, J.A. Bonacin, R.R. Passos, L.A. Pocrifka, Mater. Res. **18**(3), 639–643 (2015)
41. J.P. Singh, W.C. Lim, S.O. Won, J. Song, K.H. Chae, J. Korean Phys. Soc. **72**(8), 890–899 (2018)
42. R. Tailor, A. Ahmadalinezhad, A. Sayari, Chem. Eng. J. **240**, 462–468 (2014)
43. R. Tailor, A. Sayari, Chem. Eng. J. **289**, 142–214 (2016)
44. Z. Zhang, J. Wang, L. Lang, ACS Omega **3**(11), 16369–16376 (2018)
45. P. Ammendola, F. Raganati, R. Chirone, Chem. Eng. J. **322**, 302–313 (2017)
46. D. Tiwari, C. Goel, H. Bhunia, P.K. Bajpai, Sep. Purif. Technol. **181**, 107–122 (2017)
47. S. Sumathi, S. Bhatia, K.T. Lee, A.R. Mohamed, Energy Fuels **24**(1), 427–431 (2010)
48. B. Zhou et al., J. Air Waste Manag. Assoc. **65**(2), 165–170 (2015)
49. H. Wang, D. Xie, Q. Chen, C. You, Chem. Eng. J. **303**, 425–432 (2016)
50. X. Gao et al., Chinese J. Chem. Eng. **26**, 2139–2147 (2018)
51. P. Cheng, B.J. Tatarchuk, Chem. Eng. Sci. **201**, 157–166 (2019)

52. M. Chen, X. Deng, F. He, Energy Fuels **30**(2), 1183–1191 (2016)
53. F. Rahmani, D. Mowla, G. Karimi, A. Golkhar, B. Rahmatmand, Sep. Purif. Technol. **153**, 162–169 (2015)
54. A. de Sá, A. S. Abreu, I. Moura, A. V. Machado, Water Purification, (Ed. Elsevier Inc., 2017), pp. 289–322.
55. F.O. Erdogan, Chem. Chem. Technol. **13**(2), 129–135 (2019)
56. P. Nanta, K. Kasemwong, W. Skolpap, J. Environ. Chem. Eng. **6**, 794–802 (2018)
57. N. Can, B.C. Ömür, A. Altındal, Sens. Actuators B **237**, 953–961 (2016)
58. C. Feng et al., New J. Chem. **44**(6), 2256–2267 (2020)
59. R.V. Sales et al., Catalysts **9**, 651 (2019)
60. K.L. Tan, B.H. Hameed, J. Taiwan Inst. Chem. Eng. **74**, 25–48 (2017)
61. F. Wu, R. Tseng, R. Juang, Chem. Eng. J. **153**, 1–8 (2009)
62. Y. Teng, Z. Liu, G. Xu, K. Zhang, Energies **10**, 115 (2017)